

Analysis and Optimization of Droop Controller for Microgrid System Based on Small-Signal Dynamic Model

Kai Yu, Qian Ai, *Member, IEEE*, Shiyi Wang, Jianmo Ni, and Tianguang Lv

Abstract—Droop control strategy enables the microgrid switch between grid-connected and islanded mode flexibly, and easily realizes the “plug and play” function of distributed generation and loads, which has recently aroused great concerns. However, small disturbances may occur during the changing process and eventually yield transient oscillation, thus the focus of microgrid control is how to switch smoothly within different operation modes. In order to improve the dynamic characteristics of an inverter-based microgrid, this paper derived a precise small-signal state-space model of the whole microgrid including droop controller, network, and loads. The key control parameters of the inverter and their optimum ranges, which greatly influence the damping frequency of oscillatory components in the transient response, can be obtained through eigenvalue analysis. In addition, genetic algorithm is introduced to search for optimal settings of the key parameters during time-domain simulation in MATLAB/Simulink. Simulation results verified the effectiveness of the proposed small-signal dynamic model and optimization algorithm, and enhanced the dynamic performance of the microgrid, which can be the reference for parameter design of droop control in low voltage microgrids.

Index Terms—Droop controller, microgrid, small-signal analysis, dynamic model, genetic algorithms, control optimization.

I. INTRODUCTION

WITH THE energy crisis and environmental pollution becoming more and more serious recently, the energy sector is moving into an era where main increases in electrical energy demand will be met through widespread installation of distributed generation (DG). Microgrid is an advanced operating regime for the application of DGs, which is formed into an independent control unit consisting of a cluster of DGs, controllers, energy storages and loads [1], [2]. This regime can maintain the reliability of network and solve a series of problems caused by large-scale DG access, thus become an advanced scheme for future power supply and an important part of smartgrid construction [3].

Manuscript received September 8, 2014; revised January 13, 2015, May 19, 2015, and August 24, 2015; accepted November 13, 2015. This work was supported by the National Natural Science Foundation of China under Grant 51577115. Paper no. TSG-00899-2014.

The authors are with the Department of Electrical Engineering, Shanghai Jiao Tong University, Shanghai 200240, China (e-mail: yukaiee@126.com; aqian@sjtu.edu.cn).

Color versions of one or more of the figures in this paper are available online at <http://ieeexplore.ieee.org>.

Digital Object Identifier 10.1109/TSG.2015.2501316

Microgrids can be operated in either autonomous or grid connected mode, which can freely access to the utility grid [4]. However, due to the low physical inertia of microgrid [5], the dynamic response is much quicker than the traditional rotating machines which make the system potentially susceptible to oscillation resulting from network disturbances [6]. Therefore one of the important concerns in the reliable operation of a microgrid is small-signal stability. It is quite essential to analyze the small-signal model and select different parameters of controller or filter, in order to maintain power quality within the regulated range and enhance the dynamic performance. The stability analysis in conventional power system is well established with the network dynamics usually neglected, however in microgrids, modeling of the complete small-signal dynamic equation for microgrids may be difficult to obtain because of complexity and diversity of the control strategy of DG. As a result, modeling and performance analysis of small-signal for microgrid has gradually become one of the concerning issues.

Previous studies show that there is a close relationship between the stability of microgrid and the parameters of power sharing by root locus or sensitivity analysis. Reference [7] developed all the sub-modules of small-signal model in the local frame of each inverter, and analysis of the system eigenvalues showed that the dominant low-frequency modes were highly sensitive to the parameters of the power sharing controller of DG. However the model is too complex and need to be simplified in practical application. Reference [8] and [9] showed the relationship between stability and affecting factors as loads droop gain, and the equivalent line impedance. But it only obtained the regular pattern of parameters variation and did not put forward any specific optimization scheme. Reference [10] employed particle swarm optimization algorithm to search for the optimal settings of the control parameters for microgrids, however the searching constraint is difficult to determine without analysis of small-signal model. Reference [11] proposed Particle Swarm Optimization(PSO) algorithms for the droop controllers of inverter-interfaced DGs by dynamic model, but it only considered the impact of PI controller parameters, thus results were not comprehensive and still needed further improvement.

In addition, the control strategies for microgrid are various, and have their own small-signal model to embody the steady-state and dynamic performance. By analyzing the small-signal

model, proper parameters will be chosen to fulfill better stability and dynamics. Control of microgrids in both two modes can be classified into three kinds, PQ control, V/f control and droop control. Reference [12] and [13] presented that the droop control could be applied to both two modes, ensuring that all DGs have the same position and achieve the reasonable distribution of load without communication, which avoided transient oscillation during the switch of operation modes and realized the "plug and play" function of DG. In recent years, researches on droop control in both AC and DC microgrids have been conducted with the goal of equal power sharing and less circulating current. Several control strategies have been adopted, such as the double-layer hierarchical control strategy [14], the adaptive droop control method based on droop index [15] and the three-layer droop control method [16] in dc microgrids. Reference [17] proposed a novel droop control strategy that considers the impact of complex impedance condition to achieve accurate power sharing. Reference [18] came up with a virtual flux droop method to achieve lower frequency deviation.

In this paper, the small-signal dynamic modeling of droop controller for the whole microgrid is derived and improved, and then genetic algorithm (GA) is used to optimize the operation characteristics of the microgrid. The remainder of this paper is organized as follows. Section II presents a typical microgrid structure based on droop control. In Section III, modeling of inverter, network, and load is presented and a complete microgrid small-signal equation is obtained. In Section IV, the relationship between the stability, power sharing dynamic performance and parameters are analyzed by using eigenvalue analysis, meanwhile optimization domain is calculated. Section VI proposes the optimization objective function and GA optimization procedure during dynamic switching process. In Section VII, evaluation results in Simulink are provided to demonstrate the effectiveness of the proposed small-signal model and optimization scheme. Conclusions are drawn in Section VIII.

II. MICROGRID SYSTEM BASED ON DROOP CONTROL

Emulating the principle of the governor of a conventional synchronous generator, droop control can achieve accurate power sharing between different DGs to balance sudden disturbances through the linear droop characteristic of frequency to active power ($f - P$) and voltage magnitude to reactive power ($u - Q$). The controller is formed by three loops: 1) power-sharing control, used to set the frequency and magnitude for the fundamental voltage of the inverter according to the droop coefficients; 2) voltage control, yield close control of the output voltage and synthesize the reference current vector; and 3) inner current control, rapidly response to the filter-inductor current, reject high frequency disturbances and generate voltage vector signal to pulse-width modulation (PWM) module [19].

A typical microgrid discussed in this paper is shown in Fig. 1. It contains two DGs which are all assumed to be DC source, on account of that most kinds of energy sources such as wind or solar can be considered as DC source after

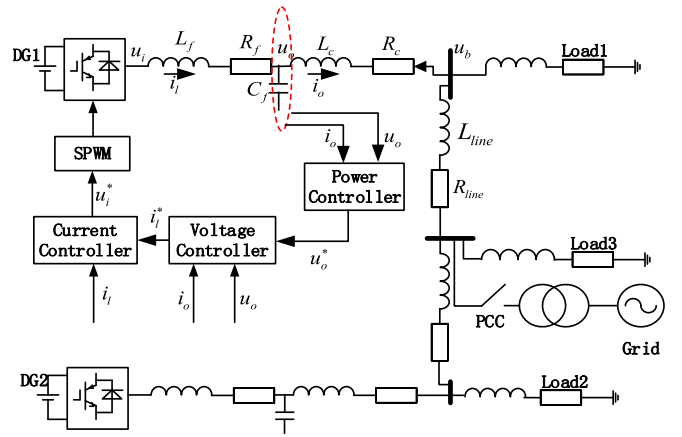


Fig. 1. Microgrid equivalent circuit and control structure.

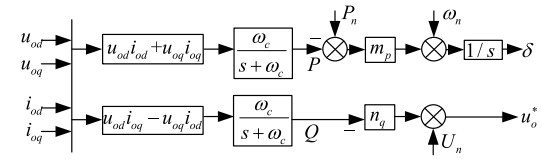


Fig. 2. Block diagram of power controller.

rectification. Every DG connects a local static load through a three-leg inverter, LC filter L_f and C_f , and coupling inductor L_c , then connects to the AC bus with common load through line impedance R_{line} and L_{line} . When the Point of Common Coupling (PCC) connecting the AC bus and utility grid is off, the microgrid will operate in autonomous mode.

III. MICROGRID SMALL-SIGNAL MODELING

In this section, the microgrid shown as blocks in Fig. 1 are analyzed and expressed in terms of mathematical equations. These equations are nonlinear and need to be linearized around an operating point to form the small-signal model and study the system stability.

The small-signal dynamic model of the whole microgrid system is divided into three major sub-modules: paralleled inverters, network, and loads [20]. We will firstly build the small-signal model of the sub-modules separately and then combine them to obtain the model of the whole system.

A. Droop-Controlled Inverters and Interface Circuit

DG units are commonly interfaced to the microgrid network by voltage-source three-phase bridge inverter (VSI), output LC filter and coupling inductor. Neglecting the effect of its high switching frequency, the droop controller of a VSI consists of three parts, power sharing controller, voltage and current close-loop controller. The dynamic model of each part is derived as follows respectively.

1) *Power Controller Modeling:* The basic idea of power sharing function is to balance any increase in the load by decreasing the frequency and voltage amplitude of the system according to the droop characteristics. As shown in Fig. 2.

The instantaneous active power and reactive power are calculated from the measured output voltage and current through

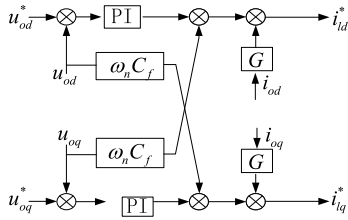


Fig. 3. Block diagram of voltage controller.

the two-axis theory. To achieve high power quality, the average powers corresponding to the fundamental component are obtained by means of a low-pass filter:

$$\begin{cases} P = \frac{\omega_c}{s + \omega_c} (u_{od} i_{od} + u_{oq} i_{oq}) \\ Q = \frac{\omega_c}{s + \omega_c} (u_{od} i_{oq} - u_{oq} i_{od}) \end{cases} \quad (1)$$

where ω_c represents the cut-off frequency of low-pass filter; s is the Laplace transform factor; u_{od} , u_{oq} , i_{od} and i_{oq} are the output voltages and currents in the dq reference frame. Thus the small-signal dynamic model of power control is given by:

$$\begin{cases} \Delta \dot{P} = -\omega_c \Delta P + \omega_c (I_{od} \Delta u_{od} + I_{oq} \Delta u_{oq} + U_{od} \Delta i_{od} + U_{oq} \Delta i_{oq}) \\ \Delta \dot{Q} = -\omega_c \Delta Q + \omega_c (I_{oq} \Delta u_{od} - I_{od} \Delta u_{oq} - U_{oq} \Delta i_{od} + U_{od} \Delta i_{oq}) \end{cases} \quad (2)$$

In paralleled inverter system, the fundamental voltage and frequency are set by the droop gain, which can be defined as:

$$\begin{cases} \omega = \omega_n - m_p (P - P_n) \\ u_{od}^* = U_n - n_q Q \\ u_{oq}^* = 0 \end{cases} \quad (3)$$

where m_p , n_q are the static droop gains. The small-signal models of the frequency and voltage in two-axis are:

$$\begin{cases} \Delta \omega = -m_p \Delta P \\ \Delta u_{od}^* = -n_q \Delta Q \\ \Delta u_{oq}^* = 0 \end{cases} \quad (4)$$

In order to convert all the variables from each inverter reference to a common frame, the angle difference between the d - q frame of each inverter and common D - Q frame is defined as:

$$\delta = \int (\omega - \omega_{com}) dt \quad (5)$$

where ω_{com} is the angular frequency of common frame taken by the first inverter usually. The small-signal model is:

$$\Delta \dot{\delta} = \Delta \omega - \Delta \omega_{com} = -m_p \Delta P - \Delta \omega_{com} \quad (6)$$

2) *Voltage Controller Model:* The voltage control loop employs a standard proportional and integral (PI) regulator which compares the sampled output voltage with the reference value given by power controller, and obtains a feed-forward gain to compensate for output current disturbances and generates the reference decoupling current vector as shown in Fig. 3.

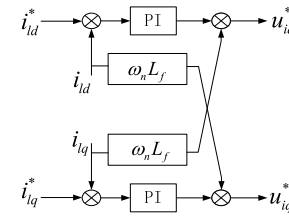


Fig. 4. Block diagram of current controller.

The corresponding state equations are:

$$\begin{cases} \frac{d\phi_d}{dt} = u_{od}^* - u_{od} \\ \frac{d\phi_q}{dt} = u_{oq}^* - u_{oq} \end{cases} \quad (7)$$

$$\begin{cases} i_{ld}^* = K_{iu} \phi_d + K_{pu} (u_{od}^* - u_{od}) - \omega_n C_f u_{oq} + G i_{od} \\ i_{lq}^* = K_{iu} \phi_q + K_{pu} (u_{oq}^* - u_{oq}) + \omega_n C_f u_{od} + G i_{oq} \end{cases} \quad (8)$$

where K_{pu} , K_{iu} are the proportional and integral gains of voltage, respectively; C_f is the per-phase capacitance of LC filter; G is the feed-forward control gain. The small-signal model of voltage control can be given by:

$$\begin{cases} \Delta \dot{\phi}_d = \Delta u_{od}^* - \Delta u_{od} \\ \Delta \dot{\phi}_q = \Delta u_{oq}^* - \Delta u_{oq} \end{cases} \quad (9)$$

$$\begin{cases} \Delta i_{ld}^* = K_{iu} \Delta \phi_d + K_{pu} \Delta u_{od}^* - K_{pu} \Delta u_{od} \\ \Delta i_{lq}^* = K_{iu} \Delta \phi_q + K_{pu} \Delta u_{oq}^* + \omega_n C_f \Delta u_{od} \\ \quad - K_{pu} \Delta u_{oq} + G \Delta i_{oq} \end{cases} \quad (10)$$

3) *Current Controller Model:* Similar to the voltage control loop, the current controller yield minimum current error by using a PI controller to compare the current sampled filter current and reference value given by voltage controller as shown in Fig. 4 and then generate the SPWM signal. The small-signal model of voltage control is:

$$\begin{cases} \Delta \dot{y}_d = \Delta i_{ld}^* - \Delta i_{ld} \\ \Delta \dot{y}_q = \Delta i_{lq}^* - \Delta i_{lq} \end{cases} \quad (11)$$

$$\begin{cases} \Delta u_{id}^* = K_{ic} \Delta y_d + K_{pc} \Delta i_{ld}^* - K_{pc} \Delta i_{ld} \\ \Delta u_{iq}^* = K_{ic} \Delta y_q + K_{pc} \Delta i_{lq}^* + \omega_n L_f \Delta i_{ld} - K_{pc} \Delta i_{lq} \end{cases} \quad (12)$$

where K_{pc} , K_{ic} are the proportional and integral gains of current, respectively; i_{ld} , i_{lq} are the filter currents in dq reference frame; L_f is the per-phase inductance.

4) *LC Filter and Coupling Inductance Model:* The inverter connected to the grid by LC filter and coupled inductor can remove the harmonic wave near the switch frequency. The linearized small-signal model is:

$$\begin{cases} \Delta \dot{i}_{ld} = -\frac{R_f}{L_f} \Delta i_{ld} + \omega_o \Delta i_{lq} - \frac{1}{L_f} \Delta u_{od} + \frac{1}{L_f} \Delta u_{id} + I_{ld} \Delta \omega \\ \Delta \dot{i}_{lq} = -\omega_o \Delta i_{ld} - \frac{R_f}{L_f} \Delta i_{lq} - \frac{1}{L_f} \Delta u_{oq} + \frac{1}{L_f} \Delta u_{iq} - I_{ld} \Delta \omega \end{cases} \quad (13)$$

$$\begin{cases} \Delta \dot{u}_{od} = \frac{1}{C_f} \Delta i_{ld} + \omega_o \Delta u_{oq} - \frac{1}{C_f} \Delta i_{od} + U_{oq} \Delta \omega \\ \Delta \dot{u}_{oq} = \frac{1}{C_f} \Delta i_{lq} - \omega_o \Delta u_{od} - \frac{1}{C_f} \Delta i_{oq} - U_{od} \Delta \omega \end{cases} \quad (14)$$

$$\begin{cases} \Delta \dot{i}_{od} = \frac{1}{L_c} \Delta u_{od} - \frac{R_c}{L_c} \Delta i_{od} + \omega_o \Delta i_{oq} - \frac{1}{L_c} \Delta u_{bd} + I_{oq} \Delta \omega \\ \Delta \dot{i}_{oq} = \frac{1}{L_c} \Delta u_{oq} - \omega_o \Delta i_{od} - \frac{R_c}{L_c} \Delta i_{oq} - \frac{1}{L_c} \Delta u_{bq} - I_{od} \Delta \omega \end{cases} \quad (15)$$

where u_{bd} , u_{bq} are the dq axis bus voltages; u_{id} , u_{iq} are the inverter voltages in dq frame respectively ; ω_o , I_{ld} , I_{lq} , U_{od} , U_{oq} , I_{od} , I_{oq} is steady state value at the initial operating point.

5) *Complete Model of the DG Interface:* Output variables i_{odq} and input variables u_{bdq} can be transferred to the common DQ frame using the transformation matrix presented below:

$$[i_{oDQ}] = [T][i_{odq}] = \begin{bmatrix} \cos(\delta) & -\sin(\delta) \\ \sin(\delta) & \cos(\delta) \end{bmatrix} [i_{odq}] \quad (16)$$

$$[u_{bdq}] = [T^{-1}][u_{bdQ}] = \begin{bmatrix} \cos(\delta) & \sin(\delta) \\ -\sin(\delta) & \cos(\delta) \end{bmatrix} [u_{bdQ}] \quad (17)$$

Linearizing the formula above:

$$\begin{aligned} [\Delta i_{oDQ}] &= \begin{bmatrix} \cos(\delta_o) & -\sin(\delta_o) \\ \sin(\delta_o) & \cos(\delta_o) \end{bmatrix} [\Delta i_{odq}] \\ &+ \begin{bmatrix} -I_{od} \sin(\delta_o) - I_{oq} \cos(\delta_o) \\ I_{od} \cos(\delta_o) - I_{oq} \sin(\delta_o) \end{bmatrix} [\Delta \delta] \end{aligned} \quad (18)$$

$$\begin{aligned} [\Delta u_{bdq}] &= \begin{bmatrix} \cos(\delta_o) & \sin(\delta_o) \\ -\sin(\delta_o) & \cos(\delta_o) \end{bmatrix} [\Delta u_{bdQ}] \\ &+ \begin{bmatrix} -U_{bd} \sin(\delta_o) + U_{bQ} \cos(\delta_o) \\ -U_{bd} \cos(\delta_o) - U_{bQ} \sin(\delta_o) \end{bmatrix} [\Delta \delta] \end{aligned} \quad (19)$$

Combining the state-space models shown in equations (2)-(19), choose the following thirteen state variables, a complete 13-order small-signal state space equation and output equation of a single inverter unit in common frame can be obtained as followed, which can be a standard inverter model:

$$[\Delta \dot{x}_{inv_i}] = A_{INV_i} [\Delta x_{inv_i}] + B_{INV_i} [\Delta u_{bdQi}] + B_{i\omega com} [\Delta \omega_{com}] \quad (20)$$

$$\begin{bmatrix} \Delta \omega_i \\ \Delta i_{oDQi} \end{bmatrix} = \begin{bmatrix} C_{INV\omega_i} \\ C_{INVci} \end{bmatrix} [\Delta x_{inv_i}] \quad (21)$$

where $[\Delta x_{inv_i}] = [\Delta \delta_i \ \Delta P_i \ \Delta Q_i \ \Delta \phi_{di} \ \Delta \phi_{qi} \ \Delta \gamma_{di} \ \Delta \gamma_{qi} \ \Delta i_{ldi} \ \Delta i_{lqi} \ \Delta u_{odi} \ \Delta u_{oqi} \ \Delta i_{odi} \ \Delta i_{oqi}]^T$, as seen on the top of the next page;

6) *Combined Model of Two Parallel Inverters:* Based on the model of individual inverter shown in (20) and (21), the small-signal model for two parallel inverters shown in Fig. 1 can be derived as:

$$\begin{aligned} [\Delta \dot{x}_{INV}] &= A_{INV} [\Delta x_{INV}] + B_{INV} [\Delta u_{bdQ}] \\ [\Delta i_{oDQ}] &= C_{INVc} [\Delta x_{INV}] \end{aligned} \quad (22)$$

where $[\Delta x_{INV}] = [\Delta x_{inv1} \ \Delta x_{inv2}]^T$ $[\Delta u_{bdQ}] = [\Delta u_{bdQ1} \ \Delta u_{bdQ2}]^T$

$$\begin{aligned} A_{INV} &= \begin{bmatrix} A_{INV1} + B_{1\omega com} C_{INV\omega_1} & A_{INV2} \\ B_{2\omega com} C_{INV\omega_1} & A_{INV2} \end{bmatrix}; \\ B_{INV} &= \begin{bmatrix} B_{INV1} & B_{INV2} \end{bmatrix}; C_{INVc} = \begin{bmatrix} C_{INVc1} & C_{INVc2} \end{bmatrix} \end{aligned}$$

Compared to the parallel model proposed in [8], we notice that the state matrix model A_{INV} is different, as shown

in (23). In [8], each inverter is modeled on its individual reference frame. However, the state equations of the network and the loads are represented on the reference frame of one of the individual inverters. This reference frame is considered as the common reference frame. In this case, the other inverters need to be translated to this common reference frame. While in this paper, we choose the first inverter's output angular frequency as the common angular frequency of the whole system, that is to say $\Delta \omega_{com} = \Delta \omega_1 = C_{INV\omega_1} \Delta x_{inv1}$. Therefore the state matrix is easier to be established because the transformation work is largely bypassed. The state matrix model A_{INV} presented in (22) has coupling items, which is more intuitive and precise to describe the certain effects that the common inverter's state variables have on the other inverters. Meanwhile $C_{INV\omega_2}$ doesn't need to be calculated in A_{INV} of the new model, which greatly reduces the amount of calculation especially in the microgrid containing lots of DGs.

$$A_{INV} = \begin{bmatrix} A_{INV1} + B_{1\omega com} C_{INV\omega_1} & A_{INV2} + B_{2\omega com} C_{INV\omega_2} \end{bmatrix} \quad (23)$$

B. Network and Load Model

For the microgrid shown in Fig. 1, the small-signal model of network can be derived similar to the LC filter linearization process presented before, so the model in DQ frame is:

$$[\Delta \dot{i}_{lineDQ}] = A_{NET} [\Delta i_{lineDQ}] + B_{1NET} [\Delta u_{bDQ}] + B_{2NET} \Delta \omega \quad (24)$$

$$[\Delta \dot{i}_{loadDQ}] = A_{LOAD} [\Delta i_{loadDQ}] + B_{1LOAD} [\Delta u_{bDQ}] + B_{2LOAD} \Delta \omega \quad (25)$$

where:

$$A_{NET} = \begin{bmatrix} -\frac{R_{line1}}{L_{line1}} & \omega_o & & \\ -\omega_o & -\frac{R_{line1}}{L_{line1}} & -\frac{R_{line2}}{L_{line2}} & \omega_o \\ & & -\omega_o & -\frac{R_{line2}}{L_{line2}} \end{bmatrix};$$

$$B_{1NET} = \begin{bmatrix} \frac{1}{L_{line1}} & -\frac{1}{L_{line1}} & -\frac{1}{L_{line1}} & \\ \frac{1}{L_{line1}} & \frac{1}{L_{line1}} & \frac{1}{L_{line1}} & -\frac{1}{L_{line2}} \\ & & \frac{1}{L_{line2}} & -\frac{1}{L_{line2}} \\ & & \frac{1}{L_{line2}} & -\frac{1}{L_{line2}} \end{bmatrix};$$

Since the coefficient matrix of load model is almost the same as network model above, it is not mentioned here.

C. Complete Microgrid Model

To well define the input variables u_{bdQ} , a large enough virtual resistor r_N is assumed between each node and ground,

$$\begin{aligned}
A_{INV_i} = & \begin{bmatrix} 0 & -m_p \\ 0 & -\omega_c \\ 0 & 0 & -\omega_c \\ 0 & 0 & -n_q \\ 0 & 0 & 0 \\ 0 & 0 & -n_q K_{pu} & K_{iu} & -1 & -K_{pu} & -\omega_n C_f & G & 0 \\ 0 & 0 & 0 & 0 & 0 & -1 & -K_{pu} & 0 & G \\ 0 & -m_p I_{lq} & \frac{-n_q K_{pu} K_{pc}}{L_f} & \frac{K_{iu} K_{pc}}{L_f} & 0 & \frac{-K_{pc} - R_f}{L_f} & \omega_o - \omega_n & -\frac{K_{pu} K_{pc} - 1}{L_f} & \frac{K_{pc} G}{L_f} & 0 \\ 0 & m_p I_{ld} & \frac{K_{iu} K_{pc}}{L_f} & 0 & \frac{K_{ic}}{L_f} & \omega_n - \omega_o & \frac{-K_{pc} - R_f}{L_f} & \frac{\omega_n C_f K_{pc}}{L_f} & \frac{-K_{pu} K_{pc} - 1}{L_f} & \frac{K_{pc} G}{L_f} \\ 0 & -m_p U_{oq} & & & \frac{1}{C_f} & 0 & 0 & \omega_o & -\frac{1}{C_f} & 0 \\ 0 & m_p U_{od} & & & \frac{1}{C_f} & -\omega_o & 0 & 0 & -\frac{1}{C_f} & 0 \\ \frac{U_{bD} \sin \delta_o - U_{bQ} \cos \delta_o}{L_c} & -m_p I_{oq} & & & & \frac{1}{L_c} & 0 & -\frac{R_c}{L_c} & \omega_o & \\ \frac{U_{bD} \cos \delta_o + U_{bQ} \sin \delta_o}{L_c} & m_p I_{od} & & & & & \frac{1}{L_c} & -\omega_o & -\frac{R_c}{L_c} & \end{bmatrix}; \\
B_{INV_i} = & \begin{bmatrix} 0 & \dots & 0 & -\frac{\cos \delta_o}{L_c} & -\frac{\sin \delta_o}{L_c} \\ 0 & \dots & 0 & \frac{\sin \delta_o}{L_c} & -\frac{\cos \delta_o}{L_c} \end{bmatrix}_{2 \times 13}^T; \quad B_{i\omega com} = [-1 \quad 0 \quad \dots \quad 0]_{1 \times 13}^T; \\
C_{INV\omega i} = & \begin{cases} [0 \quad -m_p \quad 0 \quad \dots \quad 0]_{1 \times 13} & i = 1 \\ [0 \dots 0]_{1 \times 13} & i \neq 1 \end{cases}; \\
C_{INVci} = & \begin{bmatrix} -I_{od} \sin \delta_o - I_{oq} \cos \delta_o & 0 & \dots & 0 & \cos \delta_o & -\sin \delta_o \\ I_{od} \cos \delta_o - I_{oq} \sin \delta_o & 0 & \dots & 0 & \sin \delta_o & \cos \delta_o \end{bmatrix}_{2 \times 13};
\end{aligned}$$

which can reduce the impact on dynamic stability of the system. The small-signal model of node is given by:

$$[\Delta u_{bDQ}] = R_N(M_{INV}[\Delta i_{oDQ}] + M_{LOAD}[\Delta i_{loadDQ}] + M_{NET}[\Delta i_{lineDQ}]) \quad (26)$$

where M_{INV} maps the DG connection points onto microgrid network nodes, M_{LOAD} maps load connection points onto nodes, M_{NET} maps the connecting lines onto nodes. Fig. 1 consists of $s=2$ DG, $n=2$ lines, $p=3$ loads, $m=3$ nodes, thus:

$$\begin{aligned}
R_N = & \begin{bmatrix} r_N & & \\ & \ddots & \\ & & r_N \end{bmatrix}_{2m \times 2m}; \quad M_{INV} = \begin{bmatrix} 1 & & \\ & 1 & \\ 0 & 0 & 0 & 0 \\ 0 & 0 & 0 & 0 \\ & & & 1 \\ & & & 1 \end{bmatrix}_{2m \times 2s}; \\
M_{LOAD} = & \begin{bmatrix} -1 & & \\ & \ddots & \\ & & -1 \end{bmatrix}_{2m \times 2p}; \\
M_{NET} = & \begin{bmatrix} -1 & & \\ 0 & -1 & \\ 1 & 0 & -1 \\ & 1 & 0 & -1 \\ & & 1 & 0 \\ & & & 1 \end{bmatrix}_{2m \times 2n};
\end{aligned}$$

Based on equations (22)-(26), we can get the whole complete $(2n + 2p + 13s) = 36$ order small-signal

model of Fig. 1:

$$\begin{bmatrix} \Delta \dot{x}_{INV} \\ \Delta \dot{i}_{lineDQ} \\ \Delta \dot{i}_{loadDQ} \end{bmatrix} = A_{sys} \begin{bmatrix} \Delta x_{INV} \\ \Delta i_{lineDQ} \\ \Delta i_{loadDQ} \end{bmatrix} \quad (27)$$

where A_{sys} is shown in Appendix A.

IV. EIGENVALUE ANALYSIS

In order to obtain the initial steady state operating point conditions of the microgrid system in Fig. 1, a test model of the system is implemented in MATLAB/Simulink. System parameters and initial operating values of each variable are given in Appendix table A1 and A2. Based on the linearized small signal model presented in Section II, the complete eigenvalue spectrum of the system state matrix A_{sys} can be calculated under the initial conditions, as shown in Fig. 5. It can be seen that the frequency of these eigenvalues are distributed in three clusters. The analysis shows that the low-frequency eigenvalues near the imaginary axis are the most dominant and crucial for system stability, while the eigenvalues close to the real axis will affect the dynamic performance and damping properties of the system [21], [22].

Here, active and reactive power coefficient m_p , n_q are changed respectively, the root locus of dominant eigenvalues are shown as Fig. 6 and Fig. 7. When m_p is small, several pairs of complex-conjugate roots are far from the imaginary axis, then the system can be equivalent to a first order system without overshoot, however its dynamic response time is very long and steady-state error exist. With m_p increases,

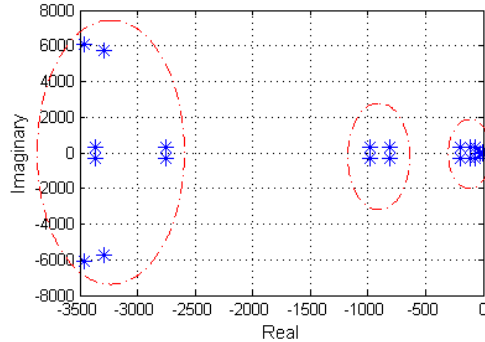
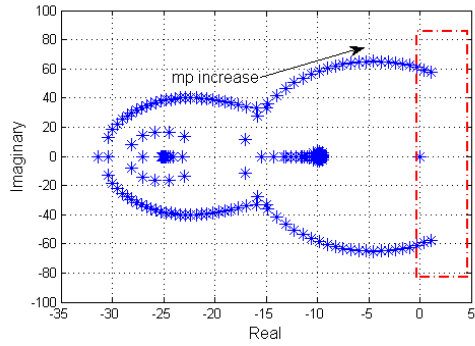
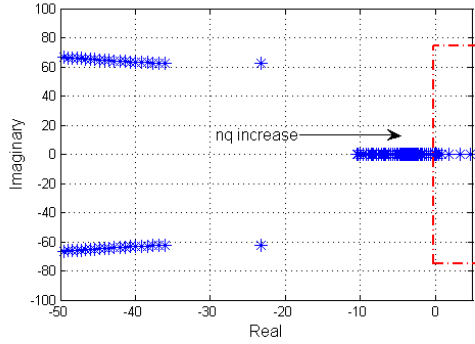
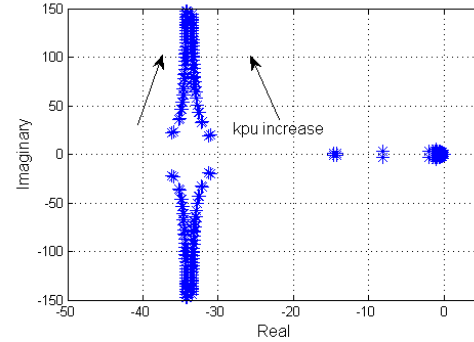
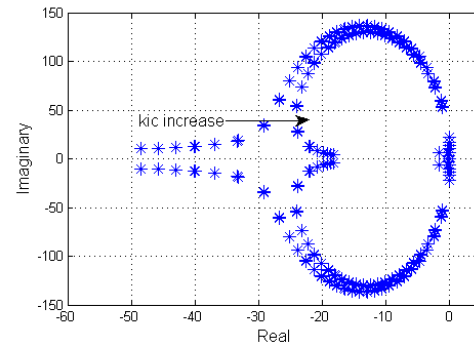
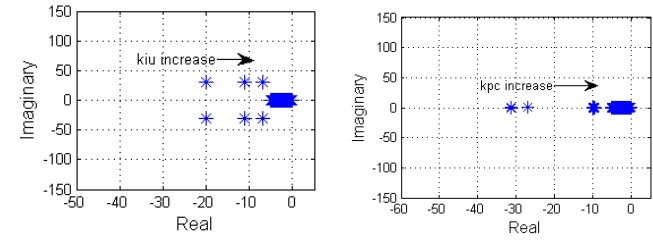


Fig. 5. Eigenvalue spectrum of microgrid state matrix.

Fig. 6. Dominant root locus as $m_p \in [1e-7, 1e-2]$.Fig. 7. Dominant root locus as $n_q \in [1e-7, 1e-2]$.

the dominant eigenvalues gradually move away from the real axis improving the dynamic performance, meanwhile close to the imaginary axis which decrease the damping ratio of the system and become unstable. Fig. 7 shows n_q has little influence on the dynamic performance of the system, but when the value is too large, the dominant roots move toward unstable region, making the system more oscillatory, and eventually yield instability.

On the other hand, changing the proportional and integral parameters of PI controller in voltage loop and current loop respectively, we find that proportional parameter of voltage loop K_{pu} , and integral parameter of current loop K_{ic} have a great influence on the dominant eigenvalues. The root locus is shown in Fig. 8 and Fig. 9. While the integral parameters of voltage loop K_{iu} and proportional parameter of current loop

Fig. 8. Dominant root locus as $K_{pu} \in [0, 50]$.Fig. 9. Dominant root locus as $K_{ic} \in [0, 50]$.Fig. 10. Dominant root locus as the $K_{iu}, K_{pc} \in [1, 1000]$.TABLE I
OPTIMIZATION DOMAIN OF MAIN PARAMETERS

Parameter	Value Domain
m_p	[4e-6, 8.7e-5]
n_q	[1e-5, 7.3e-4]
K_{pu}	[1, 23.2]
K_{ic}	[0, 0.9]

K_{pc} doesn't affect the dominant root significantly in the range of [1,1000], as shown in Fig. 10, which can be ignored.

To sum up, the key parameters affecting the microgrid stability and dynamic performance are mainly four factors m_p , n_q , K_{pu} and K_{ic} . Their value domain can be obtained from the critical value of the root locus, which can greatly improve the following computational efficiency for the optimization algorithm and ensure the realization of the optimization objective. Optimization domain is shown in Tab. I.

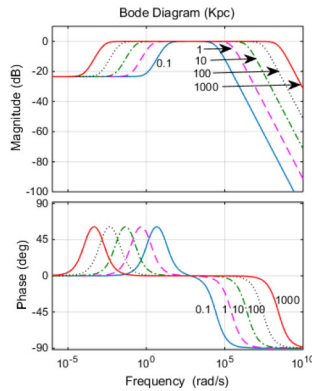


Fig. 11. Frequency response curve of current loop.

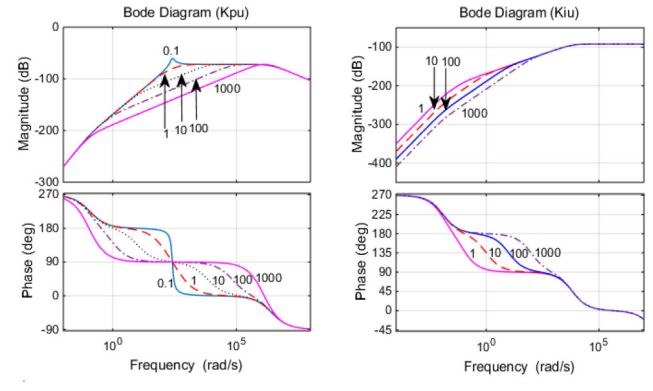
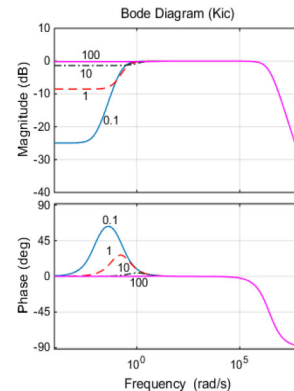


Fig. 12. Frequency response of output impedance of the closed-loop voltage controller.

V. FREQUENCY DOMAIN VERIFICATION

To verify the correctness of the optimization domain of proportional and integral parameters of PI controllers in voltage and current loop, we compare and analyze the frequency domain characteristics of different parameters. The frequency response curve of current loop is shown in Fig. 11. When the current loop proportional parameter K_{pc} moves in the range of [1,1000], the magnitude and phase gain remain nearly 0 at $f=50\text{Hz}$, which means the output current closely follows the input reference current and the current loop operates well with K_{pc} in the range of [1,1000]. However, in order to achieve better dynamics, the bandwidth should be greater to decrease response time, however, the magnitude gain should be small in high frequency to remove harmonics. As a compromise, we choose 10 as the value of K_{pc} . As for the integral parameter K_{ic} , in the optimization domain [0,0.9] obtained from root locus analysis, the output current also follows the input reference current. Besides, the current loop can have a greater bandwidth and faster response rate with K_{ic} in the optimization domain.

Fig. 12 are the frequency domain characteristics of the voltage controller output impedance, which is closely related to the PI parameters in voltage loop. The droop control method implements under the condition that the reactance of the circuit is larger than the resistance. As a result, the inverter equivalent output impedance should be reactive. When integral parameter K_{iu} changes in the range of [1,1000], the phase gain falls in [90,100] at $f=50\text{Hz}$, which means the equivalent output impedance is reactive. In order to suppress harmonics, the reactive bandwidth should not be too large, so we choose 100 as the value of K_{iu} . When the proportional parameter K_{pu} changes in optimization domain [1,23.2], the phase gain falls in [80,90] at $f=50\text{Hz}$, which means the optimization domain of K_{pu} sufficiently satisfies this requirement. Besides, with K_{pu} in the optimization range, the reactive bandwidth of equivalent output impedance is relatively low, which can help remove the high frequency harmonics.

The frequency domain characteristics of control loops verified the correctness of the PI parameters obtained from root locus analysis and determine the value of K_{pc} and K_{iu} .

VI. MICROGRID CONTROL AND OPTIMIZATION BASED ON GENETIC ALGORITHM

As microgrid can switch between grid-connected mode and islanded mode, we need to establish a reasonable objective function to ensure the stability and smooth switching of different operation mode. Considering that output power of DG is an important indicator of system performance, we can take the integral of deviation between the instantaneous power and the nominal power in different operation mode under disturbances as the optimization objective function to represent the dynamic performance, and try to minimize the integral value, which means the power can quickly response to the change of nominal power, and be stabilized without big overshoot during the switching process. The objective function can be expressed as:

$$\min J = \sum_{i=1}^M \left\{ \int_{t=t_0^i}^{t_f^i} (t - t_0^i) \left[(P(t) - P^*(t))^2 + (Q(t) - Q^*(t))^2 \right] dt \right\} \quad (28)$$

where M is the number of operation mode for microgrid; t_0^i , t_f^i is the start and termination time in operation mode i .

Since the objective function is not differentiable, the conventional mathematical optimization methods are not available to solve the problem. Genetic algorithm is a modern heuristic algorithm by simulating biological genetic and evolutionary process [23], [24]. GA is an iterative process. A set of potential solutions are kept and allowed to reproduce in each generation. They are selected according to the fitness value and copied over into the next generation by mutation and crossover, and the process repeats. After a certain rounds of evolution, the global optimal solutions can be discovered with great probability.

With the characteristics of parallel, stochastic, global search and adaptive, GA is exactly suitable for solving complex nonlinear optimization problem. Choosing microgrid control parameters $X = [m_p, n_q, K_{pu}, K_{ic}]$ as optimal variables, the final optimal control is implemented by combining Simulink and MATLAB platform as shown in Fig. 13.

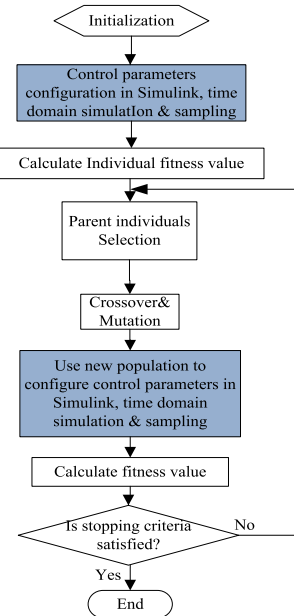


Fig. 13. Flowchart of microgrid operation optimization of genetic algorithm.

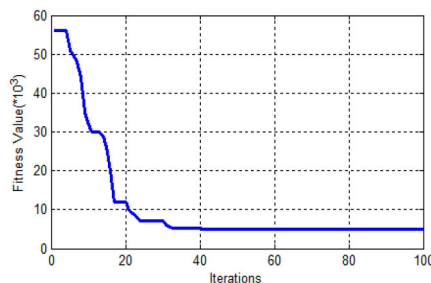
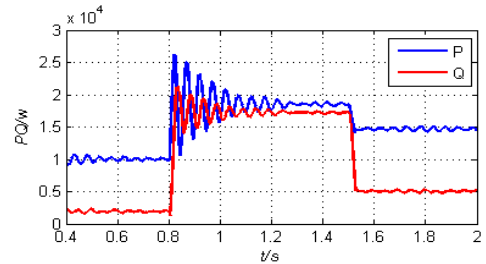
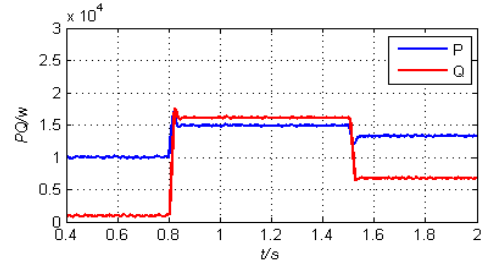
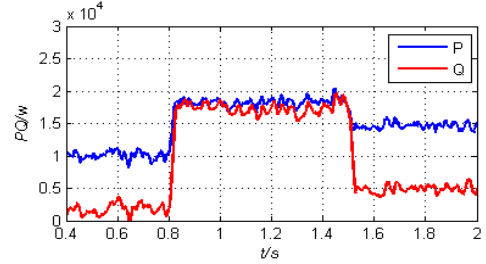
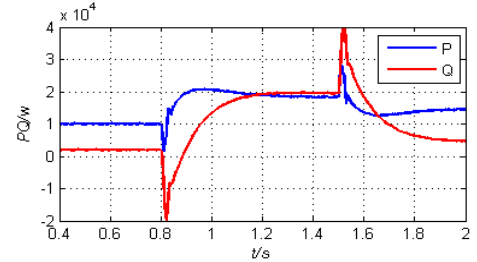


Fig. 14. Convergence curve of objective function.

VII. SIMULATION RESULTS

To evaluate the performance of the proposed control optimization strategy, the microgrid model is implemented for both mode transition and abrupt load change simulation under the Matlab/Simulink environment. The simulation sequence is: 1) 0-0.8s, the system operates in grid connected mode. 2) 0.8-1.5s, breaks the PCC so that the microgrid switches to the island mode. 3) 1.5-2s, suddenly cuts off the public Load3. The initial population size is set to 40, initial crossover probability is 0.7, mutation probability is 0.01, and maximum generation is 100. This offline optimization method obtains the self-adaptive time step to accelerate the speed at first and converge to the optimal solution gradually. Fig. 14 presents the convergence process of the objective function, from which we can see the objective function reaches the minimum after 40th generation. The final optimization result is $[m_p, n_q, K_{pu}, K_{ic}] = [1.03e^{-5}, 2.95e^{-4}, 10.11, 0.12]$.

Since the microgrid absorbs some power from the grid at initial steady-state conditions, the output power of DG will increase when the system switches to autonomous mode after $t=0.8$, then decrease after the load is cut off. Using the optimal parameters obtained from the GA optimization procedure mentioned above, the responses of power are compared before

Fig. 15. Power response of DG1 as m_p is beyond domain before optimization.Fig. 16. Power response of DG1 as n_q is beyond domain before optimization.Fig. 17. Power response of DG1 as K_{pu} is beyond domain before optimization.Fig. 18. Power response of DG1 as K_{ic} is beyond domain before optimization.

and after optimization. Fig. 15-18 show the active and reactive power sharing performance of DG1 units when the parameters m_p , n_q , K_{pu} , K_{ic} are separately beyond domain before optimization. We can see that the parameters setting improperly may affect the dynamic performance of microgrid to some extent, and lead to large transient response or power oscillation during the mode transition periods, which may overload the unit and activate the unit protection. After the optimization of all parameters, the power response of DG1 and DG2 in Simulink is shown in Fig. 19, which notices that the response to the change is fast and without significant overshoot, meanwhile settling time is improved.

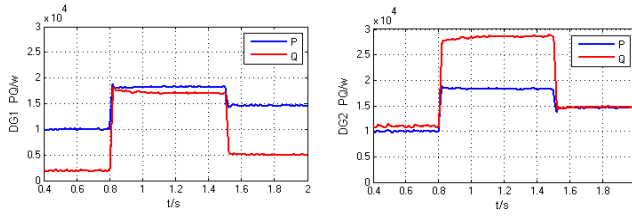


Fig. 19. Power response of DG1 and DG2 after optimization (simulation results).

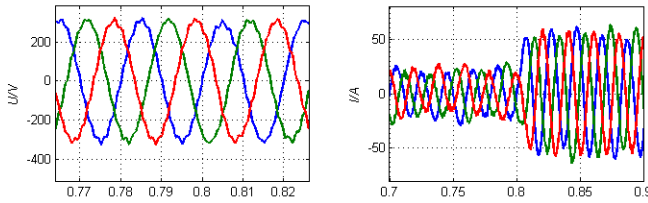


Fig. 20. Voltage and currents wave forms of K_{pu} before optimization.

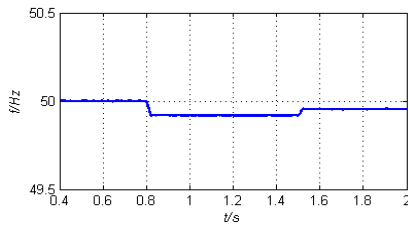


Fig. 21. AC bus frequency after optimization.

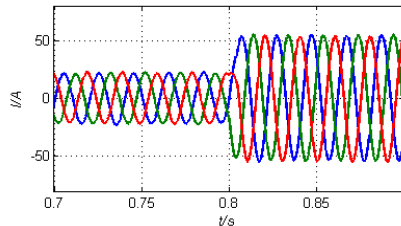


Fig. 22. Current magnification of DG1 after optimization.

Fig. 20 shows voltage and currents wave forms of K_{pu} before optimization, from which we can see that there exist distortion in the three-phase voltage and current curve, especially that the current has serious harmonic. Fig. 21 shows the system frequency variations after optimization which are well maintained around the nominal values. Fig. 22 is the partial view of optimized DG1 output current at switching process, which shows that the system has excellent flow characteristics.

Fig. 23 presents the power response of DG1 and DG2 obtained from the small-signal model depicted by (27), which correspond to the simulation results with the same step change in load and the network. We can observe that the system is correctly represented by the small-signal model.

In droop control mode, the output active power of the inverter is directly related to the frequency of the microgrid and droop gain m_p . Since the frequency is the same in the system and inverters have the equal real power droop gain m_p ,

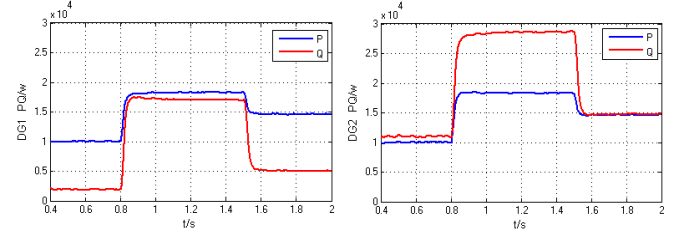


Fig. 23. Power response of DG1 and DG2 after optimization (small-signal results).

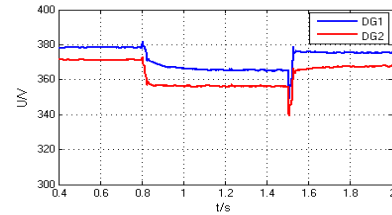


Fig. 24. Output voltage of DG1 and DG2.

unbalanced power is evenly distributed to inverters of DG1 and DG2. As for the distribution of reactive power, since bus voltages are different in the microgrid, the output reactive power can be unequal even though the reactive droop gain n_q is equal between the inverters. DG1 has no reactive power load connected directly while DG2 has reactive power load of 20kvar connected directly. According to the principle that reactive power should be compensated by the nearest source or compensator, DG2 should output more reactive power to meet the demand of load2 and the public load while the output reactive power of DG2 mainly meet the demand of the public load, as Fig. 19 illustrate. Hence, the output voltage of DG2 is lower than that of DG1. Fig. 24 shows that output voltages of the inverters basically keeps smooth and varies because of the change of output reactive power.

The value of the parameters are chosen from the value domain obtained from the root locus analysis. According to the simulation results, the minimum power damping during the switch between different working modes and the lowest oscillation during the steady-state operation has been achieved, which means the proposed control optimization approach closely matches the small-signal analysis and the system stability and the dynamic performance are improved.

VIII. CONCLUSION

To solve the dynamic response problem in operation mode switching of microgrid, this paper developed a detailed and precise small-signal state-space model of a microgrid based on droop control strategy, including inverter dynamics, network and load dynamics, then combined with a common reference frame to obtain the complete model. Using eigenvalue analysis, it is demonstrated that system's small-signal stability and performance are highly sensitive to such affecting parameters as power droop gain m_p , n_q , proportional parameter of voltage K_{pu} , and integral parameter of current K_{ic} , meanwhile the reasonable optimization domain of the four parameters is obtained by the root locus and verified

TABLE AI
SYSTEM PARAMETERS OF MICROGRID

Parameter	Values	Parameter	Values
L_f	1.5e-3 H	m_p	1.03e-5
R_f	0.15 Ω	n_q	2.95e-4
C_f	1500e-6 F	K_{pu}	10.11
L_c	0.5e-3 H	K_{iu}	100
R_c	0.05 Ω	K_{pc}	10
R_{line1}	0.147 Ω	K_{ic}	0.12
L_{line1}	1.63e-3 H	G	0.7
R_{line2}	0.11 Ω	ω_c	31.4 rad/s
L_{line2}	1.25e-3 H		

TABLE AII
INITIAL OPERATING VALUES

Parameter	Values	Parameter	Values
U_{od}	[311.2 311.6] V	I_{lined1}	-7.8 A
U_{oq}	[0 0] V	I_{lineq1}	1.4 A
I_{od}	[21.2 21.2] A	I_{lined2}	-5.3 A
I_{oq}	[-0.34 -1.05] A	I_{lineq2}	0.7 A
I_{ld}	[21.2 21.2] A	U_{bd}	[308.7 308.5 308] V
I_{lq}	[-14.3 -11.3] A	U_{bq}	[-2.8 -1.3 -1.5] V
δ_o	[0 1.9e-3] rad	ω_o	314 rad/s

by frequency domain characteristics analysis, which greatly improves the computational efficiency of the introduced GA process.

Simulation results in Matlab/Simulink validate the four parameters from small-signal analysis do have key effects on stability and dynamic performance under load disturbances, and demonstrate the effectiveness of the proposed GA approach which improves the microgrid dynamic performance. As a result, the proposed control optimization scheme significantly contributes to preserve microgrid stability and parameter selection of low voltage network.

APPENDIX

$$A_{sys} = \begin{bmatrix} A_{INV} + B_{INV}R_NM_{INV}C_{INVc} & B_{1NET}R_NM_{INV}C_{INVc} + B_{2NET}C_{INV\omega} \\ B_{1LOAD}R_NM_{INV}C_{INVc} + B_{2LOAD}C_{INV\omega} & \begin{matrix} B_{INV}R_NM_{NET} & B_{INV}R_NM_{LOAD} \\ B_{1NET}R_NM_{NET} & B_{1NET}R_NM_{LOAD} \\ B_{1LOAD}R_NM_{NET} & A_{LOAD} + B_{1LOAD}R_NM_{LOAD} \end{matrix} \end{bmatrix}$$

REFERENCES

- [1] T. L. Vandoorn, J. C. Vasquez, J. De Kooning, J. M. Guerrero, and L. Vandervelde, "Microgrids: Hierarchical control and an overview of the control and reserve management strategies," *IEEE Ind. Electron. Mag.*, vol. 7, no. 4, pp. 42–55, Dec. 2013.
- [2] N. Hatziargyriou, H. Asano, R. Iravani, and C. Marnay, "Microgrids," *IEEE Power Energy Mag.*, vol. 5, no. 4, pp. 78–94, Jul./Aug. 2007.
- [3] A. Iapkchi and F. Albuyeh, "Grid of the future," *IEEE Power Energy Mag.*, vol. 7, no. 2, pp. 52–62, Mar./Apr. 2009.
- [4] A. G. Tsikalakis and N. D. Hatziargyriou, "Centralized control for optimizing microgrids operation," *IEEE Trans. Energy Convers.*, vol. 23, no. 1, pp. 241–248, Mar. 2008.
- [5] R.-F. Yuan, Q. Ai, and X. He, "Research on dynamic load modelling based on power quality monitoring system," *IET Gener. Transm. Distrib.*, vol. 7, no. 1, pp. 46–51, Jan. 2013.
- [6] Y. Li and Y. W. Li, "Power management of inverter interfaced autonomous microgrid based on virtual frequency-voltage frame," *IEEE Trans. Smart Grid*, vol. 2, no. 1, pp. 30–40, Mar. 2011.
- [7] N. Pogaku, M. Prodanovic, and T. C. Green, "Modeling, analysis and testing of autonomous operation of an inverter-based microgrid," *IEEE Trans. Power Electron.*, vol. 22, no. 2, pp. 613–625, Mar. 2007.
- [8] Z. X. Xiao, C. S. Wang, and S. X. Wang, "Small-signal stability analysis of microgrid containing multiple micro sources," *Autom. Elect. Power Syst.*, vol. 33, no. 6, pp. 81–85, 2009.
- [9] F. Katiraei, M. R. Iravani, and P. W. Lehn, "Small-signal dynamic model of a micro-grid including conventional and electronically interfaced distributed resources," *IET Gener. Transm. Distrib.*, vol. 1, no. 3, pp. 369–378, May 2007.
- [10] M. A. Hassan and M. A. Abido, "Optimal design of microgrids in autonomous and grid-connected modes using particle swarm optimization," *IEEE Trans. Power Electron.*, vol. 26, no. 3, pp. 755–769, Mar. 2011.
- [11] I.-Y. Chung, W. Liu, D. A. Cartes, E. G. Collins, Jr., and S.-I. Moon, "Control methods of inverter-interfaced distributed generators in a microgrid system," *IEEE Trans. Ind. Appl.*, vol. 46, no. 3, pp. 1078–1088, May/Jun. 2010.
- [12] Y. A.-R. I. Mohamed and E. F. El-Saadany, "Adaptive decentralized droop controller to preserve power sharing stability of paralleled inverters in distributed generation microgrids," *IEEE Trans. Power Electron.*, vol. 23, no. 6, pp. 2806–2816, Nov. 2008.
- [13] E. Barklund, N. Pogaku, M. Prodanovic, C. Hernandez-Aramburo, and T. C. Green, "Energy management in autonomous microgrid using stability-constrained droop control of inverters," *IEEE Trans. Power Electron.*, vol. 23, no. 5, pp. 2346–2352, Sep. 2008.
- [14] T. Dragicevic, J. M. Guerrero, J. C. Vasquez, and D. Skrlec, "Supervisory control of an adaptive-droop regulated DC microgrid with battery management capability," *IEEE Trans. Power Electron.*, vol. 29, no. 2, pp. 695–706, Feb. 2014.
- [15] S. Augustine, M. K. Mishra, and N. Lakshminarasamma, "Adaptive droop control strategy for load sharing and circulating current minimization in low-voltage standalone DC microgrid," *IEEE Trans. Sustain. Energy*, vol. 6, no. 1, pp. 132–141, Jan. 2015.
- [16] L. Meng, T. Dragicevic, J. C. Vasquez, and J. M. Guerrero, "Tertiary and secondary control levels for efficiency optimization and system damping in droop controlled DC-DC converters," *IEEE Trans. Smart Grid*, vol. 6, no. 6, pp. 2615–2626, Nov. 2015.
- [17] W. Yao, M. Chen, J. Matas, J. M. Guerrero, and Z.-M. Qian, "Design and analysis of the droop control method for parallel inverters considering the impact of the complex impedance on the power sharing," *IEEE Trans. Ind. Electron.*, vol. 58, no. 2, pp. 576–588, Feb. 2011.
- [18] J. Hu, J. Zhu, D. G. Dorrell, and J. M. Guerrero, "Virtual flux droop method—A new control strategy of inverters in microgrids," *IEEE Trans. Power Electron.*, vol. 29, no. 9, pp. 4704–4711, Sep. 2014.
- [19] S. V. Iyer, M. N. Belur, and M. C. Chandorkar, "A generalized computational method to determine stability of a multi-inverter microgrid," *IEEE Trans. Power Electron.*, vol. 25, no. 9, pp. 2420–2432, Sep. 2010.
- [20] P. E. S. N. Raju and T. Jain, "Small signal modelling and stability analysis of an islanded AC microgrid with inverter interfaced DGs," in *Proc. Int. Conf. IEEE Smart Elect. Grid (ISEG)*, Guntur, India, 2014, pp. 1–8.
- [21] M. Rasheduzzaman, J. Mueller, and J. W. Kimball, "An accurate small-signal model of inverter-dominated islanded microgrids using reference frame," *IEEE J. Emerg. Sel. Topics Power Electron.*, vol. 2, no. 4, pp. 1070–1080, Dec. 2014.
- [22] S. Anand and B. G. Fernandes, "Reduced-order model and stability analysis of low-voltage DC microgrid," *IEEE Trans. Ind. Electron.*, vol. 60, no. 11, pp. 5040–5049, Nov. 2013.
- [23] J. Q. Puma and D. G. Colome, "Parameters identification of excitation system models using genetic algorithms," *IET Gener. Transm. Distrib.*, vol. 2, no. 3, pp. 456–467, May 2008.
- [24] A. E. Eiben and J. E. Smith, *Introduction to Evolutionary Computing*. Berlin, Germany: Springer-Verlag, 2003.



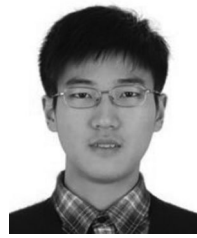
Kai Yu received the Bachelor's degree in electrical engineering from Shandong University, Shandong, in 2014. He is currently pursuing the Master's degree with the School of Electronic Information and Electrical Engineering, Shanghai Jiao Tong University, Shanghai, China.

His research interests include microgrids, energy Internet, and intelligent algorithms.



Shiyi Wang received the Bachelor's degree in automation from Tongji University, Shanghai, China, in 2012. She is currently pursuing the Master's degree in electrical engineering with the Department of Electronic Information and Electrical Engineering, Shanghai Jiao Tong University, China.

Her research interests include intelligent algorithms, microgrids, and application of power electronics.



Jianmo Ni received the B.S. degree from Shanghai Jiao Tong University, China, in 2013, and the M.S. degree from Waseda University, Japan, in 2014. He is currently pursuing the M.S. degree with Shanghai Jiao Tong University. Since 2012, he has been attending the Dual-Master Program of Shanghai Jiao Tong University and Waseda University. His research interests include smart grid, game theory, and computer-aided design in very large-scale integration.



Qian Ai received the Bachelor's degree from Shanghai Jiao Tong University, Shanghai, China, in 1991; the Master's degree from Wuhan University, in 1994; and the Ph.D. degree from Tsinghua University, in 1999, all in electrical engineering.

He was with Nanyang Technological University, Singapore, for one year, and the University of Bath, U.K., for two years. He then returned to Shanghai Jiao Tong University, where he is currently a Professor with the School of Electronic Information and Electrical Engineering. His main interests include power quality, load modeling, smart grids, microgrid, and intelligent algorithms.



Tianguang Lv received the Bachelor's degree in electrical engineering from Shandong University, Shandong, in 2013. He is currently pursuing the Master's degree with the School of Electronic Information and Electrical Engineering, Shanghai Jiao Tong University, Shanghai, China.

His research interests include microgrid, distributed generation, and intelligent algorithms.